Role of the Interactions between the Active Site Base and the Substrate Schiff Base in Amine Oxidase Catalysis. Evidence from Structural and Spectroscopic Studies of the 2-Hydrazinopyridine Adduct of *Escherichia coli* Amine Oxidase†

Minae Mure,*,‡,§ Doreen E. Brown,|| Colin Saysell,⊥ Melanie S. Rogers,|| Carrie M. Wilmot,# Christian R. Kurtis,⊥ Michael J. McPherson,⊥ Simon E. V. Phillips,⊥ Peter F. Knowles,*,⊥ and David M. Dooley*,||

Department of Chemistry, The University of Kansas, Lawrence, Kansas 66045, Department of Chemistry, University of California, Berkeley, California 94720, Department of Chemistry and Biochemistry, Montana State University, Bozeman, Montana 59717, Astbury Centre for Structural Molecular Biology, School of Biochemistry and Molecular Biology, University of Leeds, Leeds LS2 9JT, United Kingdom, and Department of Biochemistry, Molecular Biology, and Biophysics, University of Minnesota, Minneapolis, Minnesota 55455

Received September 17, 2004; Revised Manuscript Received November 4, 2004

ABSTRACT: 2-Hydrazinopyridine (2HP) is an irreversible inhibitor of copper amine oxidases (CAOs). 2HP reacts directly at the C5 position of the TPQ cofactor, yielding an intense chromophore with λ_{max} ~430 nm (adduct **I**) in *Escherichia coli* amine oxidase (ECAO). The adduct **I** form of wild type (WT-ECAO) was assigned as a hydrazone on the basis of the X-ray crystal structure. The hydrazone adduct appears to be stabilized by two key hydrogen-bonding interactions between the TPQ−2HP moiety and two active site residues: the catalytic base (D383) and the conserved tyrosine residue (Y369). In this work, we have synthesized a model compound (**2**) for adduct **I** from the reaction of a TPQ model compound (**1**) and 2HP. NMR spectroscopy and X-ray crystallography show that **2** exists predominantly as the azo form (λ_{max} at 414 nm). Comparison of the UV−vis and resonance Raman spectra of **2** with adduct **I** in WT, D383E, D383N, and Y369F forms of ECAO revealed that adduct **I** in WT and D383N is a tautomeric mixture where the hydrazone form is favored. In D383E adduct **I**, the equilibrium is further shifted in favor of the hydrazone form. UV−vis spectroscopic pH titrations of adduct **I** in WT, D383N, D383E, and **2** confirmed that D383 in WT adduct **I** is protonated at pH 7 and stabilizes the hydrazone tautomer by a short hydrogen-bonding interaction. The deprotonation of D383 (pK_a ~ 9.7) in adduct **I** resulted in conversion of adduct **I** to the azo tautomer with a blue shift of the λ_{max} to 420 nm, close to that of **2**. In contrast, adduct **I** in D383N and D383E is stable and did not show any pH-dependent spectral changes. In Y369F, adduct **I** was not stable and gradually converted into a new species with λ_{max} at ~530 nm (adduct **II**). A detailed mechanism for the adduct **I** formation in WT has been proposed that is consistent with the mechanism proposed for the oxidation of substrate by CAOs but addresses some key differences in the active site chemistry of hydrazine inhibitors and substrate amines.

Copper amine oxidases (CAOs)[1] are a class of enzymes involved in the metabolism of primary amines (*1*, *2*) and are widely distributed among prokaryotic and eukaryotic organisms where the substrate specificities vary between sources. CAOs have important biological roles including nutrient catabolism in bacteria and yeast and wound healing in plants (*1*, *3*). The physiological role of CAOs in mammals is less well understood. Mammalian CAOs have been proposed to be involved in the metabolism of biogenic amines such as histamine (*4*) and, more recently, implicated in cell signaling and cell−cell adhesion (*5*).

CAOs are homodimers containing a tightly bound Cu(II) and an organic prosthetic group identified as TPQ (2,4,5-trihydroxyphenylalanine quinone or topa quinone) in each subunit (*6*). TPQ is derived from a conserved tyrosyl residue in the active site which undergoes a posttranslational modification, its biosynthesis requiring only molecular oxygen and Cu(II) (*7*−*9*). Crystal structures are available for CAOs from bacteria [*Escherichia coli*, ECAO (*10*); *Arthrobacter globiformis*, AGAO (*11*)], yeast [*Hansenula polymorpha*,

† This work was supported by grants from the National Institutes of Health (GM27659 to D.M.D.), the Biotechnology and the Biological Sciences Research Council (24/B04841, 24/B10432, and 24/B13477 to M.J.M., S.E.V.P., and P.F.K.), and the Department of Chemistry, University of Kansas (to M.M.).

* To whom correspondence should be addressed. M.M.: e-mail, mmure@ku.edu; tel, 785-864-2901; fax, 785-864-5396. P.F.K.: e-mail, P.F.Knowles@leeds.ac.uk; tel, +44 113 233-2595; fax, +44 113 233-3167. D.M.D.: e-mail, dmdooley@montana.edu; tel, 406-994-4373; fax, 406-994-7989.

‡ The University of Kansas.

§ University of California, Berkeley.

|| Montana State University.

⊥ University of Leeds.

University of Minnesota.

[1] Abbreviations: AGAO, *Arthrobacter globiformis* amine oxidase; BSAO, bovine serum amine oxidase; CAO, copper amine oxidase; ECAO, *Escherichia coli* amine oxidase; HPAO, *Hansenula polymorpha* amine oxidase; 2HP, 2-hydrazinopyridine; PPLO, *Pichia pastoris* lysyl oxidase; PSAO, pea seedling amine oxidase; PSB, product Schiff base; SSB, substrate Schiff base; rR, resonance Raman; TCP, tranylcypromine; TPQ, topa quinone (2,4,5-trihydroxyphenylalanine quinone); WT-ECAO, wild-type ECAO.

10.1021/bi047988k CCC: $30.25
Published on Web 01/11/2005

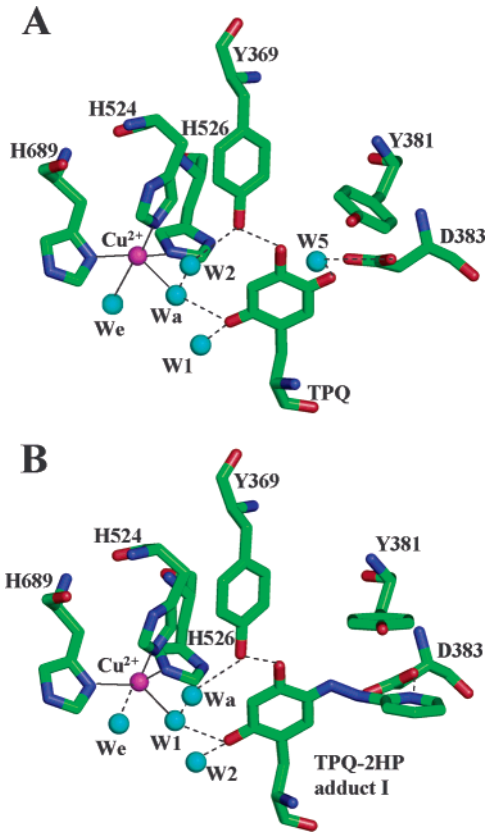

FIGURE 1: (A) Crystal structure of the active site of WT-ECAO (1DYU.pdb) and (B) crystal structure of the active site in WT-ECAO adduct **I** (1SPU.pdb). In panel A, the water molecule, W_e, was modeled into the figure on the basis of the crystal structure in ref *18*. Solid lines represent bonds to copper ligands, and dashed lines represent the hydrogen-bonding network, except for W_e in (B), where the dashed line indicates that this ligand is at a significantly longer distance than in (A).

HPAO (*12*); *Pichia pastoris*, PPLO (*13*, *14*)], and plants [pea seedling, PSAO (*15*)]. The CAO structures share a common motif having two long polypeptide arms that extend from one domain of one monomer into the active site of the other. A large β-sandwich domain contains the active site in which Cu(II) and TPQ are present. In the resting state, Cu(II) is coordinated in a distorted square-pyramidal geometry by four equatorial ligands (three conserved histidine residues and an equatorial water, W_e) and weakly by an axial water, W_a. TPQ has been detected in different orientations, depending on the conditions under which the crystals were grown and the form of CAO or active site mutant examined. It is proposed that optimal catalytic activity requires that TPQ is not directly coordinated to Cu(II) but instead lies nearby, where O2 of TPQ is hydrogen bonded to W_a, O4 of TPQ is hydrogen bonded to the hydroxyl group of a conserved tyrosine (Y369 in ECAO), and O5 of TPQ is directed toward the active site base (D383 in ECAO) and the proposed substrate entry channel as shown in Figure 1A (*16*). In the structures of active site mutants where these specific hydrogen-bonding interactions are perturbed or absent, TPQ is either disordered, rotated toward Cu(II), or bound to Cu(II) (*17*−*23*). These orientations might be correlated with significant or complete loss of catalytic activity when compared to the wild-type enzyme, depending on the rates of reorientation. Despite considerable overall structural homology among the CAOs characterized, there are considerable differences in the properties of the substrate entry channel and the solvent accessibility of TPQ (*14*, *23*, *24*). These differences could explain the broad range of substrate specificities identified among CAOs and their preference for selective mechanism-based inhibitors (*14*, *25*).

The catalytic cycle of CAOs proceeds through a ping-pong mechanism, consisting of two half-reactions as shown in Scheme 1 (*24*, *26*). In the reductive half-reaction, the oxidized form of the cofactor (TPQ_{ox}) reacts with a substrate amine to form the substrate Schiff base intermediate (SSB). The conserved active site base abstracts a proton from the C1 position of the SSB, resulting in the reduction of the quinone ring to form the product Schiff base (PSB). Hydrolysis of the PSB releases a product aldehyde, leaving the cofactor as an aminoresorcinol (TPQ_{red}). In the oxidative half-reaction, O_2 reacts with TPQ_{red} to form an iminoquinone (TPQ_{imq}) and hydrogen peroxide. Finally, TPQ_{imq} can either hydrolyze to TPQ_{ox} or react with a second molecule of substrate to form the SSB directly (transimination), where both pathways result in the release of NH_4^+.

Hydrazine derivatives such as phenylhydrazine and *p*-nitrophenylhydrazine are strong irreversible inhibitors of CAOs (*6*, *27*−*29*). These hydrazines bind covalently at the C5 position of the TPQ cofactor to produce complexes with characteristic spectroscopic properties ($\epsilon \geq 30000\ M^{-1}\ cm^{-1}$, λ_{max} 415−447 nm for the phenylhydrazine adduct, λ_{max} 457−463 nm for the *p*-nitrophenylhydrazine adduct) (*6*, *27*, *30*, *31*). These complexes are used widely to both identify and quantitate the TPQ cofactor. The original identification of TPQ as the cofactor in CAOs was achieved by direct comparison of the phenylhydrazine adduct of TPQ in bovine serum amine oxidase (BSAO) with a corresponding model compound (*6*). It was found that the UV−vis and resonance Raman (rR) spectra of the inhibited enzyme were identical with those of the model TPQ−phenylhydrazine adduct (*27*, *32*).

2-Hydrazinopyridine (2HP) was first reported to be an irreversible inhibitor of pig plasma amine oxidase (PPAO) (*33*, *34*). Early investigations with PPAO demonstrated that 2HP reacted with the quinone cofactor to form two spectroscopically distinct products: an initial adduct with a characteristic absorption band at ~420 nm (adduct **I**) that slowly converted to a final adduct with an absorption band at ~520 nm (adduct **II**) (*35*). Very different rR spectra were observed for both adducts, indicating that their structures were distinct (*35*). Similar spectroscopic changes were also observed in the reaction of 2HP with other CAOs (*35*−*37*). The conversion of adduct **I** to adduct **II** could be facilitated under a variety of conditions, although different rates of conversion were observed depending on the enzyme source. At the time, the absence of an X-ray crystal structure for any CAO and the ambiguous nature of the cofactor precluded further characterization of these two adducts.

In 1997, the structure of the 2HP-inhibited form of ECAO was solved by X-ray crystallography (*38*). 2HP was shown to covalently bind to the C5 position of the TPQ ring as expected, and the structure of the TPQ−2HP adduct (adduct **I**) was best fit as the hydrazone tautomer where the two rings (TPQ and the pyridine moiety of 2HP) are noncoplanar (Figure 1B). It was proposed that adduct **I** is an accurate representation of the SSB structure in the catalytic cycle. Key features of the structure are hydrogen-bonding interac-

Scheme 1: Catalytic Cycle of CAO

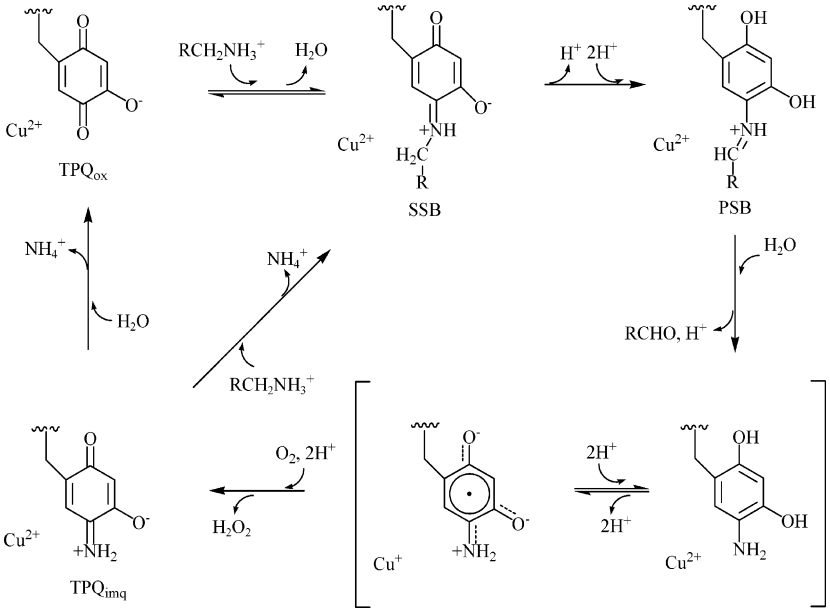

Scheme 2: Previously Proposed Mechanism for the Conversion of Adduct **I** to Adduct **II** in ECAO[a]

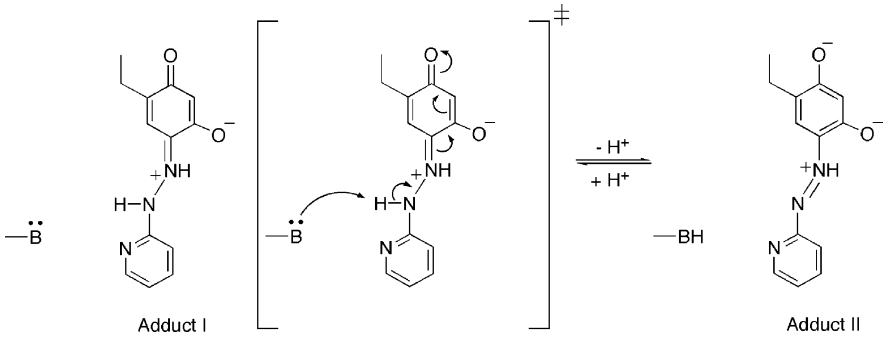

[a] See ref *36*.

tions between the N2 position of TPQ−2HP and D383 and between O4 of TPQ and the hydroxyl group of Y369. The former interaction was particularly important in supporting the assignment of D383 as the active site base involved in the catalytic cycle, although the protonation state of D383 in this complex was not clear (*38*). Site-specific mutagenesis experiments subsequently showed that D383 is critical not only for activity but also in controlling the mobility of TPQ (*17*). The adduct **I** to adduct **II** conversion has been studied as a function of pH and temperature (*36*). It was shown that adduct **I** converts to adduct **II** in a time-dependent fashion at pH ∼10. Alkaline treatment (pH 14) of adduct **I** immediately formed a species with a UV−vis spectroscopic feature similar to that of adduct **II**. Thermal incubation (60 °C) also accelerated the conversion. It was proposed that the conversion of adduct **I** to adduct **II** occurs as a result of hydrazone to azo tautomerism mediated by loss of a single proton, possibly to D383. Adduct **II** was thought to mimic the PSB complex in the catalytic cycle (Scheme 2) (*36*).

In this paper, we present a detailed spectroscopic characterization of adduct **I** in ECAO. A model compound for adduct **I** (**2**) has been synthesized and fully characterized to understand better the nature and role of the interactions which exist between the complex and the active site residues. A comparison of the structures and spectroscopic properties of adduct **I** in both the enzyme and model systems confirmed that, under physiological conditions, adduct **I** in ECAO predominantly exists as the hydrazone form whereas **2** exists as the azo form. These differences are the result of specific hydrogen bonds in the active site of CAOs that are absent in solution and also show that the original assignment of adduct **II** as the azo tautomer of TPQ−2HP is incorrect (*36*). The results have allowed us to propose a detailed mechanism for adduct **I** formation as well as illustrate the importance of the active site residues in stabilizing the hydrazone form in the enzyme over the thermodynamically more stable azo tautomer. The proposed mechanism not only helps to explain the structural differences of adduct **I** observed between the crystal structure and solution studies, but also provides key insights into the catalytic mechanism for CAOs, particularly regarding the role of the active site base (D383). The similarities and differences of the adduct **I** complex and the SSB in the catalytic cycle are addressed. Further, a structural comparison between the ECAO−2HP adduct **I**, the tranylcypromine (TCP) inhibited form of ECAO (*39*), and WT-ECAO provides key insights into how the active site pocket of ECAO has evolved to accommodate a specific conformation of the SSB intermediate to optimize the α-proton abstraction by D383. Our results demonstrate that TPQ−2HP is an important, stable, structural, and mechanistic probe for the active site of CAOs.

EXPERIMENTAL PROCEDURES

Protein Purification and Enzyme Assay. WT-ECAO and the active site base mutants of ECAO, D383E, D383N, D383A, and Y369F were prepared and purified as previously reported (*10*, *18*). The enzymes used in this study were purified to >95% homogeneity as determined by SDS−PAGE. Enzyme concentrations were determined from absorbance at 280 nm adjusted by a gravimetrically derived correction factor of 0.76 to give a concentration in milligrams per milliliter. The molar extinction coefficient at 280 nm is $\epsilon = 2.1 \times 10^5$ M^{-1} cm^{-1} (*36*). All experiments were performed aerobically. Enzyme activity was measured as previously described using a coupled assay with β-phenylethylamine as substrate (*10*).

General. UV−vis spectral studies were performed on either a Shimadzu UV2401 PC spectrophotometer or a Hewlett-Packard 8452A or a Hewlett-Packard 8450A diode array spectrophotometer equipped with a temperature-controlled cell holder at 25 ± 0.2 °C (path length of 1 cm).

UV−Vis Spectroscopic Studies and TPQ Titration with 2HP in ECAO. TPQ was titrated by stepwise additions of 0.1 molar equiv of 2HP to 1 mL of WT-ECAO in 20 mM sodium phosphate buffer at pH 7.0 ($I = 0.1$ with NaCl). The reaction was allowed to proceed until no further spectral change was detected following each addition. Absorbance changes were corrected for dilution effects. Spectral changes accompanying the addition of a 5-fold excess of 2HP (over protein concentration) to WT-ECAO, D383E, D383N, D383A, and Y369F (12.1 μM) were monitored over time. In experiments using urea, 5 μL of 2HP-derivatized D383E (0.097 mM) or D383N (0.101 mM) was diluted with 95 μL of 8 M urea (prepared in 100 mM potassium phosphate buffer, pH 7.2). WT-ECAO (0.009 mM) was prepared by the addition of a 5-fold excess of 2HP (0.045 mM) to the reaction vessel and allowed to react for 1 min before the sample (110 μL) was diluted with 490 μL of 8 M urea in 0.1 M potassium phosphate buffer, pH 7.2. The reaction was monitored for a maximum of 30 min.

UV−Vis and NMR Spectroscopic pK_a Determination of 2HP. A 10 μL aliquot of the stock solution ([2HP·HCl] = 0.18 M in water) was diluted with 990 μL of a buffer (0.02 M, $I = 0.2$ with NaCl) of the desired pH, and UV−vis spectra were recorded immediately after the dilution (final concentration = 0.18 mM). The solutions used and their pH values, measured to ±0.01, were as follows: HCl for pH <0, H_3PO_4 and NaH_2PO_4 for pH 0−3, CH_3COOH and CH_3COONa for pH 3−5.3, NaH_2PO_4 and Na_2HPO_4 for pH 5.6−7.8, $NaHCO_3$ and Na_2CO_3 for pH 8.8−10.7, Na_2HPO_4 and Na_3PO_4 for pH 10.5−11.9, and NaOH for pH >12. The pK_a values were obtained by least-squares fitting of the appropriate absorbance changes as a function of pH (see Supporting Information for the details). Details concerning the pK_a assignment of 2HP by ^{1}H and ^{15}N NMR spectroscopy are given in the Supporting Information.

*Spectroscopic pH Titration of Adduct **I** of WT-ECAO.* Titration of adduct **I** of WT-ECAO at different pHs was performed using two different protocols yielding the same result: (1) WT-ECAO (16.5 mg/mL) was allowed to react with a 2.4-fold excess of 2HP for 1 h. Spectra were recorded after addition of 15 μL of the 2HP-modified protein to 185 μL of 20 mM potassium phosphate buffer and 0.1 M NaCl prepared over a pH range from 6 to 10; (2) WT-ECAO (1 mg/mL) was incubated for 1 h with excess 2HP (1 mM) in 100 mM sodium phosphate buffer at pH 5.85. Following this, the inhibited enzyme was split into several aliquots and dialyzed overnight versus 2 L of 100 mM sodium phosphate buffer over the pH range 6−10. At higher pHs, $NaPO_4$ borax was mixed with the buffer. Spectra were subsequently recorded.

*pH Profiles of Adduct **I** Formation between WT-ECAO and 2HP.* The rates for the formation of adduct **I** in WT-ECAO were obtained by monitoring the increase in absorbance at 430 nm on an Applied Photophysics SX-17MV stopped-flow reaction analyzer. Protein concentrations ranged from 1.5×10^{-6} to 8.0×10^{-6} M. At each pH, the 2HP concentration varied from a 10-fold excess (over protein) to a 1000-fold excess. Dependence of the initial rate (k_{obsd}) on [2HP] was determined, and the results were fitted to the Michaelis−Menten equation to obtain K_{bind} at each pH. An average of five traces were taken to obtain a mean rate constant at each [2HP] used. The K_{bind} values so obtained were plotted as a function of pH and fitted by nonlinear regression to obtain the two pK_a values (Origin, Microcal). Errors for the pK_a and K_{bind} values were generated by the fitting program. The reactions conducted in the pH range of 5.14−9.14 were buffered with the following buffer solutions: 2-(*N*-morpholino)ethanesulfonic acid (Mes) (pK_a = 6.1) for the pH range of 5.5−6.7, sodium phosphate (pK_a = 7.0) for the pH range of 5.7−8.0, *N*-(2-hydroxyethyl)-piperazine-*N*′-2-ethanesulfonic acid (Hepes) (pK_a = 7.5) for the pH range 6.8−8.2, tris(hydroxymethyl)aminomethane (Tris) (pK_a = 8.08) for pH 7.1−8.9, and 2-(*N*-cyclohexylamino)ethanesulfonic acid (Ches) (pK_a = 9.3) for pH 8.6−10.0. All solutions were adjusted with sodium chloride to an ionic strength (*I*) of 0.1.

*rR Spectroscopy on Adduct **I** WT-ECAO and Mutant Proteins.* WT-ECAO, D383E, and D383N ranging between 0.048 and 0.091 mM were derivatized with a 5-fold excess (over protein concentration) of 2HP prepared in 0.1 M potassium phosphate buffer, pH 7.2. Visible spectra were recorded before and after laser irradiation. A 0.2 mM solution of the model compound (**2**) was prepared by dissolving the compound in a minimal amount of acetonitrile (<5 μL) and then further diluting the sample to 1 mL with 100 mM potassium phosphate buffer, pH 7.2. For comparison, AGAO−2HP (0.048 mM) was prepared under the same conditions as stated above. rR spectra were collected using a Coherent Innova 302 krypton laser (413.1 nm excitation) and a Spex Triplemate spectrophotometer or a McPherson 2061 spectrograph. Both instruments were equipped with liquid nitrogen cooled CCD detectors. Data were typically collected over 2−5 min at 30−40 mW. Vibrational frequencies were calibrated relative to an aspirin or an indene standard. Data analysis was carried out using GRAMS software (Thermo Galactic) and Origin (OriginLab Corp.).

*Synthesis and Characterization of Adduct **I** (**2**) in the Model System.* 2-Hydroxy-5-*tert*-butyl-1,4-benzoquinone (**1**) was prepared according to the method described previously (*40*). 2HP and 2HP·2HCl were purchased from Aldrich and used without further purification. ^{1}H and ^{13}C NMR spectra were obtained on JEOL JMN LA-400, JEOL EX-270 MHz, Bruker AM-400, and Bruker AM-500 spectrophotometers.

Table 1: Bond Length of **2**

bond	bond length (Å)
C11−N10	1.417 (1.1)[a]
N9−N10	1.285 (1.7)
N9−C5	1.374 (1.3)
C4−O4	1.337 (1.2)
C2−O2	1.340 (1.2)

[a] Estimated total bond order number in parentheses.

IR spectra were obtained on an ASI reactIR-1000 FT-IR spectrophotometer.

*Synthesis of 4-(2-Pyridylazo)-6-tert-butylresorcinol (**2**).* Compound **1** (79.1 mg, 0.44 mmol) was treated with 1.1 molar equiv of 2HP·2HCl in 7 mL of 0.1 M potassium phosphate buffer, pH 7.2, and the reaction mixture was stirred for 2 h. An orange-red precipitate was formed, collected by centrifugation, washed three times with Milli-Q water, and then freeze-dried to yield **2** (100 mg, 83% yield): ^{1}H NMR (in CD_3CN) δ 1.370 (9H, s, H8), 5.974 (1H, s, H3), 7.170 (1H, s, H3), 7.149−7.168 (1H, m), 7.665 (1H, m), 7.820 (1H, m), 8.391 (1H, m), 15.2 (1H, br s); ^{1}H NMR (in DMSO-d_6) δ 1.344 (9H, s, H8), 6.250 (1H, s, H3), 7.353 (s, H6), 7.355 (1H, dd, J_{13-14} = 7.8 Hz, J_{12-13} = 4.0 Hz, H14), 7.771 (1H, d, J_{12-13} = 8.0 Hz, H12), 7.933 (1H, dd, J_{13-14} = 7.8 Hz, J_{12-13} = 8.0 Hz, J_{13-15} = 1.6 Hz, H11), 8.522 (1H, d, J_{14-15} = 4.0 Hz, H15), 11.195 (0.8H, br s), 14.089 (0.9H, br s); ^{1}H NMR (dilute sample in CD_3OD) δ 1.358 (9H, s, H8), 7.086 (1H, s, H6), 7.127 (1H, ddd, J_{13-14} = 7.3 Hz, J_{14-15} = 4.9 Hz, J_{12-14} = 1.0 Hz, H14), 7.657 (1H, dd, J_{12-13} = 8.5 Hz, J_{12-14} = 1.0 Hz, H12), 7.833 (1H, ddd, J_{12-13} = 8.4 Hz, J_{13-14} = 7.3 Hz, J_{13-15} = 1.7 Hz, H13), 8.290 (1H, ddd, J_{14-15} = 4.9 Hz, J_{13-15} = 1.7 Hz, J_{12-15} = 0.7 Hz, H15); ^{1}H NMR (concentrated sample in CD_3OD) δ 1.408 (9H, s, H8), 7.466 (1H, s, H6), 7.351 (1H, dd, J_{13-14} = 7.1 Hz, J_{14-15} = 5.0 Hz, H14), 7.829 (1H, d, J_{12-13} = 7.9 Hz, H12), 7.959 (1H, dd, J_{12-13} = 7.9 Hz, J_{13-14} = 7.1 Hz, J_{13-15} = 1.6 Hz, H13), 8.489 (1H, d, J_{14-15} = 5.0 Hz, H15); ^{13}C NMR (in CD_3OD) δ 30.241, 35.408, 113.612, 124.126, 130.840, 134.477, 134.617, 140.261, 149.533, 160.394, 164.195, 167.856; ^{13}C NMR (in DMSO-d_6) δ 29.397, 34.039, 104.494, 110.961, 122.964, 128.320, 132.475, 132.631, 138.719, 148.888, 159.139, 163.178, 165.622; IR (KBr) 1623 (m), 1596 (m), 1504 (s), 1480 (s), 1439 (s), 1362 (m), 1313 (m), 176 (m), 1257 (m), 126 (s), 1186 (s), 144 (m), 1097 (w), 1070 (w), 1050 (w), 1019 (w), 860 (w), 819 (w), 774 (w), 737 (w).

*pH Dependence of the Reaction of 2HP and **1**.* A 10 μL aliquot of the stock solution of **1** (5 mM in 0.02 M sodium phosphate buffer at pH 6.6) was added to 940 μL of 0.02 M sodium phosphate buffer (I = 0.2 with NaCl) at the desired pH in a quartz cell. A 50 μL stock solution of 2HP ([2HP] = 0.1 M in 0.01 N HCl) was added to the cuvette to initiate the reaction. The formation of **2** was monitored at 414 nm by UV−vis spectroscopy.

*X-ray Crystallographic Structure Determination of **2**.* A crystal of **2** with dimensions 0.05 × 0.25 × 0.25 mm was isolated from recrystallization of the NMR sample in DMSO-d_6. Diffraction data were collected on a Rigaku AFC7R diffractometer with graphite monochromated Mo−Kα radiation and a rotating anode generator. The crystallographic data are summarized in Table 1. The structure was solved by direct methods (*41*) and expanded using Fourier techniques (*42*). The non-hydrogen atoms were refined anisotropically, and hydrogen atoms were included but not refined. All calculations were performed using the teXsan crystallographic software package (Molecular Structure Corp.) (*43*). The full details of the X-ray structure determination can be found in the Supporting Information.

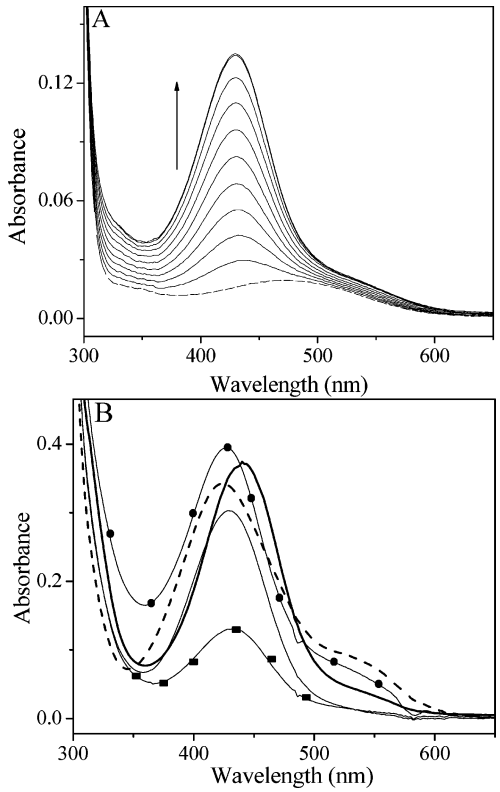

FIGURE 2: (A) Formation of adduct **I** in ECAO titrated with 0.1 molar equiv of 2HP. The protein concentration was 5.0 μM in 0.1 M sodium phosphate, pH 7.0 (I = 0.1 with NaCl). (- - -) WT-ECAO. (B) Formation of adduct **I** in WT-ECAO (●), D383E (—), Y369F (- - -), D383N (—), and D383A (■) after the addition of a 5-fold excess of 2HP. The protein concentration was 12.1 μM in 0.1 potassium phosphate, pH 7.2. WT-ECAO and Y369F spectra were recorded immediately. D393E, D383N and D393A were recorded at 1 h.

*UV−Vis Spectroscopic pK_a Determination of **2**.* A 50 μL sample of the stock solution ([**2**] = 0.83 mM in 30% methanol−water) was diluted with 950 μL of a 0.02 M (I = 0.2 with NaCl) buffer of the desired pH, and UV−vis spectra were recorded immediately after the dilution. The buffer solutions used and their pH, measured to ±0.01, were as follows: H_3PO_4 and NaH_2PO_4 for pH 0−3, CH_3COOH and CH_3COONa for pH 3−5.3, NaH_2PO_4 and Na_2HPO_4 for pH 5.6−7.8, $NaHCO_3$ and Na_2CO_3 for pH 8.8−10.7, Na_2HPO_4 and Na_3PO_4 for pH 10.5−11.9, and NaOH for pH >12.

RESULTS

*UV−Vis Spectroscopic Properties of Adduct **I** in WT and Mutants.* When WT-ECAO was treated with 2HP, a species with λ_{max} at 430 nm (adduct **I**) was observed at pH 7.0 (Figure 2A) as previously reported (*36*). The reaction was irreversible and complete after addition of ~1.3 molar equiv of 2HP. The loss of the enzyme activity correlated directly with the formation of adduct **I**. Analogous spectroscopic changes were observed when 2HP reacted with the active

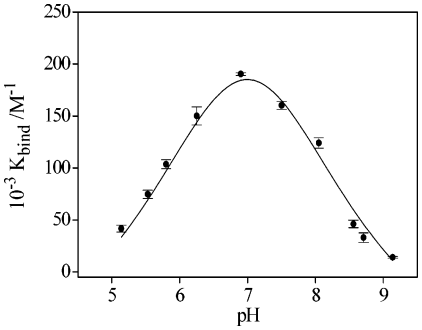

FIGURE 3: Dependence of K_{bind}, the apparent binding constant of 2HP to ECAO, on pH, $I = 0.100$ M, at 25 °C.

site base mutants D383E, D383N, and D383A,[2] as well as Y369F. Figure 2B shows the spectra of adduct **I** in WT and mutants at pH 7.2. Adduct **I** in both the WT and mutant forms of the enzyme has a red-shifted λ_{max} when compared to the model compound, **2**. Adduct **I** in WT and in D383N have a similar λ_{max} (430 nm), but the intensity of the latter absorption band is smaller. Adduct **I** in D383E shows the most red-shifted λ_{max} (440 nm). Adduct **I** in Y369F (λ_{max} = 425 nm) has an absorption spectrum closer to **2**, but it was not stable and gradually converted to adduct **II** [see the following paper (*51*)]. Note that the shoulders apparent at ~540 nm in Figure 2B are indicative of adduct **II** formation.

*Binding Kinetic Properties for Adduct **I** Formation in WT.* In a previous study, the formation of adduct **I** in WT-ECAO was shown to exhibit saturation kinetics (*17*). In the active site base mutants (D383E, D383N, and D383A), the apparent K_{bind} was greatly reduced when compared to WT, suggesting that both the charge on and the steric bulk of D383 are important for binding of 2HP. Figure 3 shows that the plot of apparent K_{bind} vs pH for WT gives a bell-shaped curve, which is best fit with pK_as of 5.8 and 8.1. These values are very close to those (5.8 and ~8) obtained from the plot of apparent K_{bind} vs pH for the formation of the adduct between the fully reversible competitive inhibitor, TCP and WT (*39*), and also from the k_{cat}/K_m vs pH plot for the oxidation of β-phenethylamine by WT-ECAO, where the lower pK_a (5.8) represents D383 and the upper pK_a (>8.0) corresponds to the substrate amine (*18*). It is unclear why the upper pK_a should be almost identical for 2HP (pK_a = 7.2 for the monoprotonated form of 2HP, as determined in this work; see Supporting Information), TCP [pK_a = 8.38 (*39*)], and β-phenethylamine [pK_a = 9.8 (*44*)] since the latter two are 1−2 pK_a units more basic than the former. Given that the pK_as of enzyme-bound 2HP, TCP, and β-phenethylamine may well differ significantly from the solution values, the similarity in the observed pK_a values may well be fortuitous. However, the results are consistent with the prevailing mechanism that requires the substrate/inhibitor be protonated and D383 be deprotonated in order for the efficient binding/reactivity to occur (Scheme 3).

*Reaction of **1** and 2HP*. To further characterize the nature of adduct **I** formed with ECAO, the reaction of a TPQ model compound (**1**) with 2HP, generating **2**, was studied by UV−vis spectroscopy. Figure 4 shows the UV−vis spectral change of the reaction of **1** and 2HP under pseudo-first-order conditions ([2HP] = 5 mM, [**1**] = 0.05 mM) at a physiological pH, 7.3. At 15 s, the characteristic absorption band of the monoanion form of **1** at 488 nm was seen. During the next 6 h, this band disappeared and a new absorption band appeared at 414 nm. The increase in absorption at 414 nm follows pseudo-first-order kinetics: $k_{obs} = k_2$[2HP] (s^{-1}) where $k_2 = 2.90 \times 10^{-5}$ (mM^{-1} s^{-1}).

The formation of the species at 414 nm was pH dependent, where the reaction rate *decreased* with increasing pH. The plot of k_{obs} vs pH, which fit the titration curve for the dissociation of a single proton, allowed the calculation of a pK_a of 7.29 ± 0.04 (see Supporting Information). The pK_a of the 4-hydroxyl group of **1** is ca. 4, and this deprotonation has been proposed to play an important role in directing the nucleophilic addition of an amine at the C-1 carbonyl carbon, as well as in mediating the stability and reactivity of reaction intermediates (*29*). The pK_as of 2HP were determined as −0.48 ± 0.05 and 7.12 ± 0.07 respectively, by UV−vis spectroscopic titration (see Supporting Information). We acquired ^{1}H and ^{15}N NMR spectral data of both the monoprotonated and the free form of 2HP in DMSO-d_6, but we were not able to unambiguously assign the origins of two pK_as in an aqueous solution (see Supporting Information). 2HP must be in its neutral form for facile nucleophilic addition to the C-1 carbonyl group of the monoanionic form of **1** in an aqueous solution. If the pK_a of 2HP controls the reaction rate, then it would be expected that the rate should increase above pH 6. However, as the rate *decreases* above pH 6, the pK_a calculated from the reaction profile cannot correspond to 2HP or to any basic group on **1** but rather must reflect the pK_a of an intermediate.

Scheme 4 shows the most plausible mechanism for formation of **2**, where the initial nucleophilic addition of 2HP to **1** is rapid and reversible, and the rate-limiting step involves protonation/dehydration of a tetrahedral carbinolamine-like intermediate, which would be subject to general acid catalysis, consistent with the observed pH dependence.

*Structure of WT-ECAO Adduct **I***. The X-ray crystal structure of WT-ECAO adduct **I** was previously determined to a resolution of 2.0 Å (*38*). Adduct **I** was assigned as the hydrazone form to reflect the ~70° rotation of the pyridine ring of the 2HP moiety with respect to the TPQ ring (Figures 1B and 5A). Resonance considerations mandate that the thermodynamically preferred conformation of both azo and hydrazone tautomers would be planar but that ring noncoplanarity can be accommodated more readily by the hydrazone tautomer. This configuration of the two rings seems to be controlled by hydrogen-bonding interactions between the pyridine nitrogen of 2HP and D383 and between O4 of the TPQ ring and Y369. It was not clear for the former whether the proton resided on the pyridine nitrogen or on the carboxylate of D383. For the latter, an oxoanion at C4 of the TPQ ring is the hydrogen bond acceptor. Further, there is a $\pi-\pi$ stacking interaction between the pyridine ring and Y381. Y381 is not strictly conserved among the CAOs so it was concluded that this $\pi-\pi$ stacking interaction is not essential for substrate/inhibitor binding (*38*). Amino acid sequence alignment of available CAOs shows that the residue corresponding to Y381 in ECAO is conserved in bacterial and mammalian forms of CAOs and replaced by phenylalanine in plant CAOs. In HPAO, Y381 aligns with an

[2] Due to the disorder of TPQ in D383A, it was difficult to titrate more than 25% of TPQ in this mutant form. For this reason, it is not possible to get a quantitative picture of how this mutant affects the formation of adduct **I**.

Scheme 3: Formation of Adduct **I** in WT-ECAO

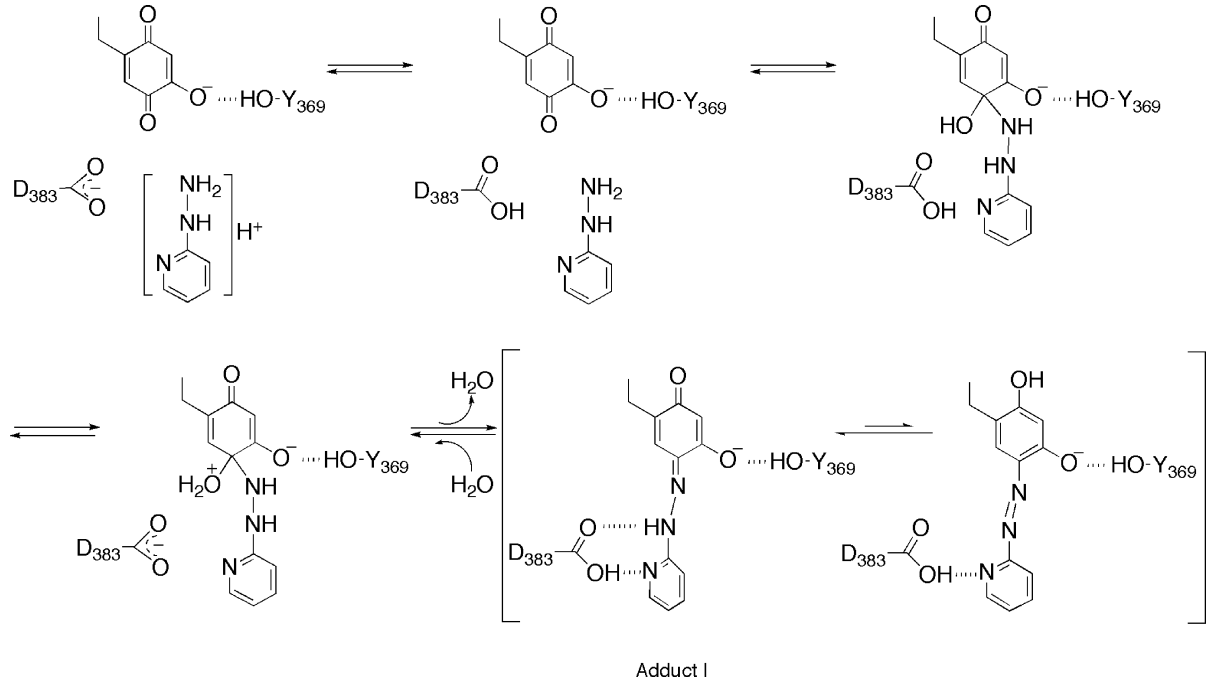

Scheme 4: Formation of **2**

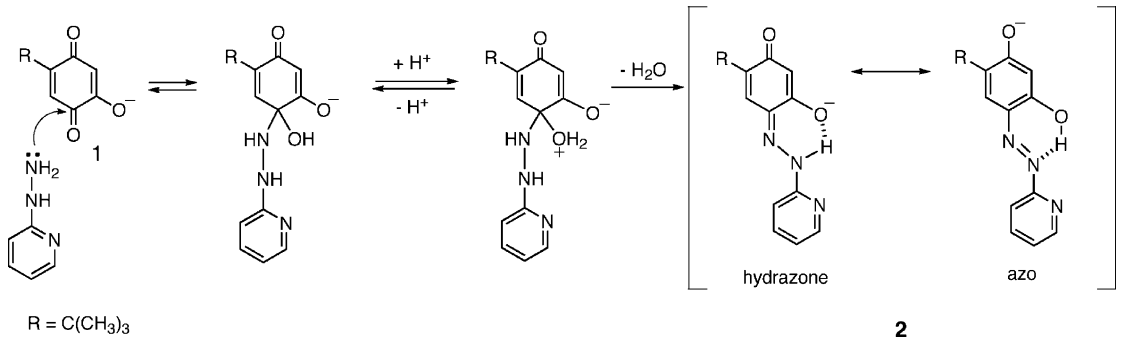

alanine (A317), but an inspection of the active site of HPAO reveals that a nearby tryptophan (W156) could provide steric bulk in place of a tyrosine or phenylalanine.

*Structure Determination of **2***. When **1** was treated with a slight molar excess of 2HP in an aqueous buffer solution at physiological pH (7.2), an orange-red precipitate was formed. The structure of the precipitate was determined to be **2** by ^{1}H and ^{13}C NMR and X-ray crystallography. The position of the nucleophilic addition has been confirmed to be at C5, the carbonyl carbon adjacent to the 4-hydroxyl group of TPQ as in the case of the *p*-nitrophenylhydrazine adduct of TPQ (*28*) and substrate Schiff base analogues (*29*).

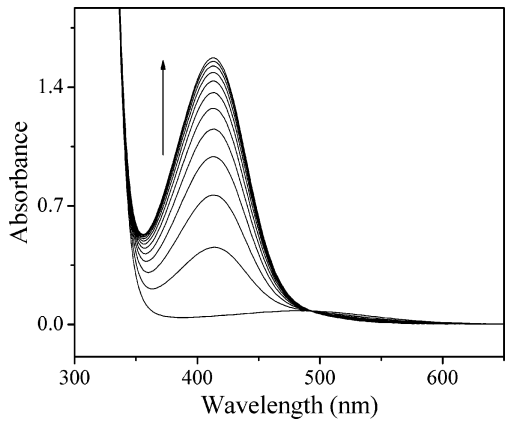

FIGURE 4: Formation of **2**. After the initial spectrum, data were recorded every 30 min for 330 min on a HP8450A diode array spectrophotometer equipped with a thermostated cell holder at 25 ± 0.2 °C (path length of 1 cm). **1** (53 μM) and 2HP (5 mM), pH 7.3.

*(a) Solution Structure of **2** Determined by NMR Spectroscopy.* Hydrazones are well-known to undergo hydrazone−azo tautomerism (see Scheme 4), and the equilibrium between the two forms is strongly influenced by the nature of the molecule, solvent, or temperature (*45*). The ^{1}H NMR spectrum of **2** indicates that it exists primarily in the azo form, in acetonitrile-d_3 and DMSO-d_6, judging from the chemical shift for the 4-hydroxyl group of the TPQ ring, which lies in the range (14−16 ppm) for a hydroxyl group hydrogen bonded to the adjacent azo group (*46*). This is in agreement with the results of ^{13}C NMR, where no signal corresponding to the carbonyl carbon (at ∼180 ppm) of the hydrazone was detected either in these solvents or in methanol-d_4. However, in methanol-d_4 and in D_2O (pH 7), rapid proton−deuterium exchange of the ring proton at C3 was observed (Scheme 5). No proton signal corresponding to H3 (5.974 ppm in acetonitrile-d_3 and 6.250 ppm in DMSO-

Scheme 5: Deuterium Exchange of the Ring Proton at the C_3 Position of **2**

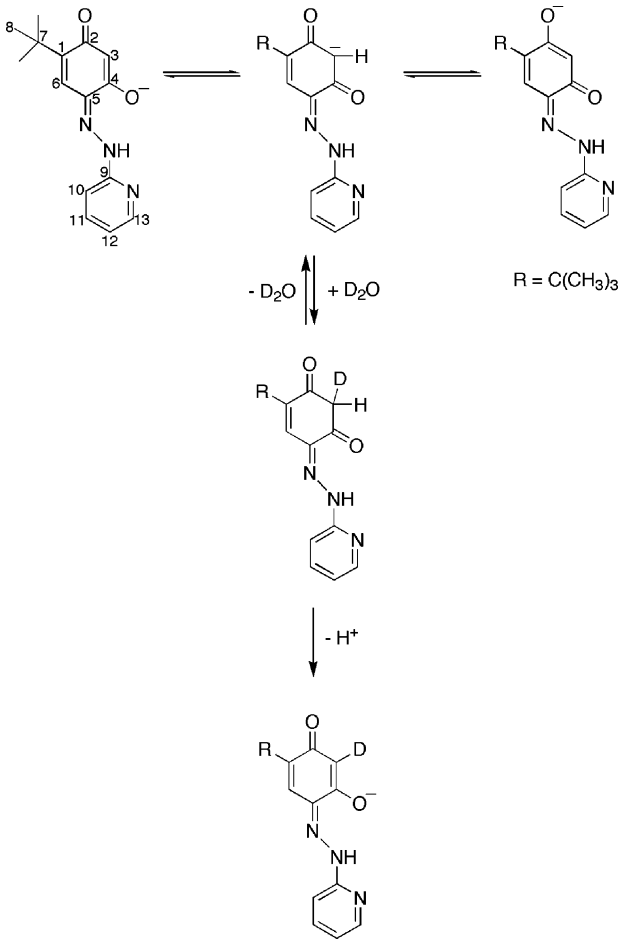

d_6) was detected, and a carbon signal at 104.494 ppm (in DMSO-d_6) became a triplet with a reduced intensity due to the exchange of H3. Intramolecular H-bonding in **2** permits a special type of interaction that is akin to resonance (*47*). Calculations on β-diketones, which contain a similar intramolecular hydrogen-bonding interaction, show that there is a single structure that is a weighted average between the keto and the enol forms. By extension, **2** can exist as an average between the hydrazone and the azo tautomers, where the negative charge is delocalized between O2 and O4, and it is this hybrid structure which undergoes C3 exchange. The rate of deuterium exchange of H3 observed for **2** was much faster than that measured for the *p*-nitrophenylhydrazine adduct of TPQ [$t_{1/2}$ for the exchange >1 h (*6*)] where this also exists predominantly as the azo form (*28*). In contrast, the exchange rate of H3 in **2** was closer to those for TPQ and its iminoquinone adduct (*40*). This would be expected if **2** exists as a resonance form that is a weighted average of the azo and hydrazone tautomers.

*(b) X-ray Crystallographic Structure Determination of **2**.* **2** crystallized as an orange prism with two molecules of **2** in the unit cell of the primitive, triclinic space group of $P\bar{1}(2)$. Although there are slight differences between the structures of the two molecules in the asymmetric unit, they are essentially identical so only one is shown in Figure 5B, and an average structure (bond lengths and angles) is discussed here (see Supporting Information). In the structure of **2**, the pyridine ring and TPQ ring are coplanar and in a

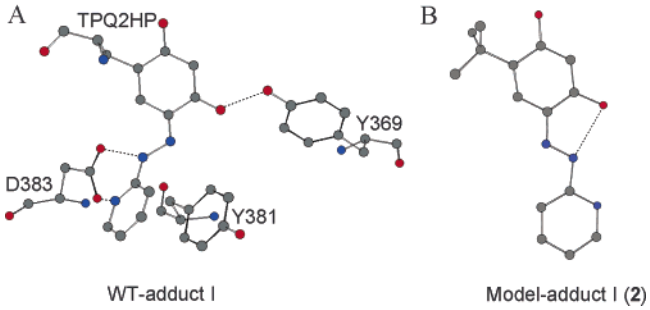

FIGURE 5: (A) Crystal structure of the TPQ-2HP moiety in WT-ECAO adduct **I**. (B) Crystal structure of **2**. Dashed lines represent hydrogen-bonding interactions.

trans conformation with respect to the azo group. The pyridine nitrogen and O4 of TPQ are in a *cis* orientation (see ECAO Adduct **I** Crystal Structure section, Figures 1B and 5A). The bond length between N1 and N2 is 1.28 Å (estimated bond order 1.8), which is a little longer than the value of the N=N bond of the aromatic azo compounds being in the range of 1.24−1.26 Å (estimated bond order 1.8−2.0). The bond length between C5 and N1 is 1.37 Å (estimated bond order 1.3). This is shorter than C−N distances of 1.41−1.46 Å for the aromatic azo compounds (estimated bond order 1.1−1.0). Both deviations indicate a structure that is a weighted average between azo (major) and hydrazone (minor) contributions. The bond length between O4 and N2 is 2.58 Å, suggesting a strong intramolecular hydrogen-bonding interaction between the 4-hydroxyl group and the azo group.

*UV−Vis Spectroscopic pH Titration of WT and Mutational Variant Forms of ECAO Adduct **I**.* As shown in Figure 6A, an increase of pH from 5.5 to 9.5 resulted in a blue shift of the λ_{max} of WT-ECAO adduct **I** from 435 nm (pH 5.5) to 420 nm (pH 9.5), where the extinction coefficient of the latter is about twice that of the former. The spectrum of WT-ECAO at pH 9.5 is very similar to that of **2** at pH 7.0 in both λ_{max} and intensity. Figure 6B shows the plot of the absorbance change at 420 nm as a function of pH, which can be fit to a single pK_a of 9.7 (the upper limit for the titration was pH ~10 as the enzyme denatures in basic solution). Similar UV−vis spectroscopic pH titrations were also performed on adduct **I** of the active site mutants (D383E and D383N) and the phenylhydrazine adduct of WT-ECAO (data not shown). There were no significant changes in the spectra of either over the pH range studied for WT-ECAO adduct **I**. These results strongly suggest that the spectral change is associated with the hydrogen-bonding interaction between the pyridine nitrogen of the 2HP moiety and D383 as indicated in the crystal structure of WT-ECAO adduct **I**. The pK_a value of 9.7 is attributed to the carboxyl group of D383, which is significantly elevated from that in the underivatized WT-ECAO (pK_a = 5.8; see above) as shown in Scheme 6. In contrast, D383N has no proton that is titratable in aqueous solution, and therefore no spectral changes should be observed over the pH range studied. In D383E, the additional CH_2 group locates the carboxyl group closer to the pyridine nitrogen, which likely results in a stronger hydrogen-bonding interaction that is less likely to be broken under pH conditions for which the enzyme is stable. Further, the very well defined electron density in the structure of D383E suggests that the TPQ is immobile and held in the productive conformation

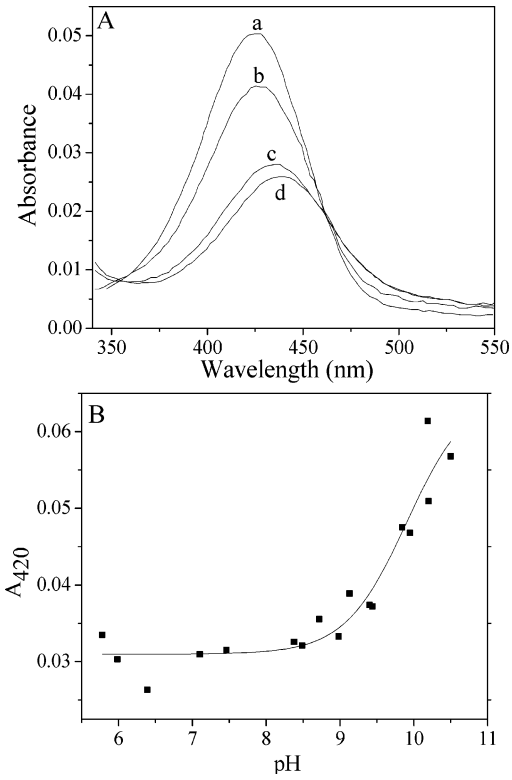

FIGURE 6: (A) Effect of pH on the UV−vis spectrum of WT-ECAO adduct **I** at the following pHs: (a) 9.48, (b) 9.00, (c) 7.60, and (d) 5.80. (B) Plot of the absorbance changes at 420 nm as a function of pH in WT-ECAO adduct **I**. Data were fit to a single pK_a of 9.70 ± 0.15.

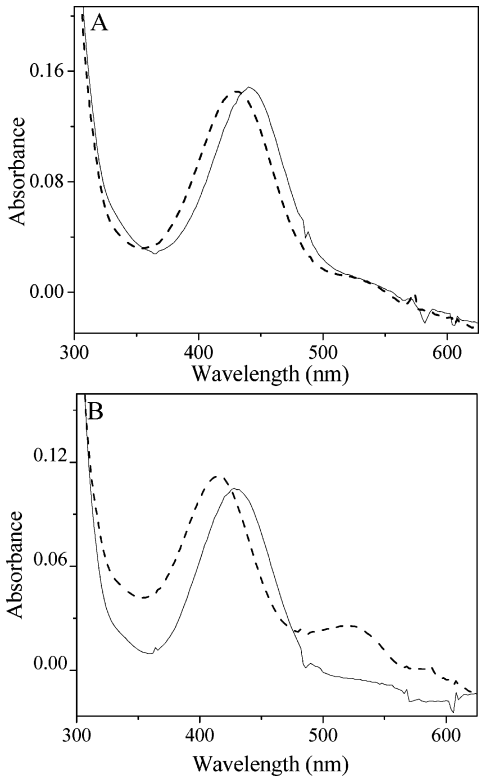

FIGURE 7: Spectral changes of adduct **I** in (A) D383E (4.9 μM) and (B) D383N (5.1 μM) after the addition of 8 M urea. (—) Hydrazone form of adduct **I**; (- - -) azo form of adduct **I**.

(*17*). To test these hypotheses, 8 M urea was added to samples of adduct **I** in WT-ECAO, D383E, and D383N in order to disrupt the hydrogen-bonding interactions in the active site by denaturation at pH 7.2. The spectral changes from the hydrazone to azo conformation were immediate in all three proteins and characterized by a ca. 15 nm blue shift in λ_{max} (Figure 7). In the case of WT-ECAO, the conversion from the hydrazone to azo proceeded much faster than with the mutant proteins even in the absence of urea. The resulting spectra are very close to that observed for WT-ECAO at pH 9.5 as well as **2** at neutral pH (Figures 6A and 4). Both λ_{max} and the line shape suggest that adduct **I** in Y369F is structurally closer to **2** (Figure 2B). However, it is not possible to perform an accurate pH titra-

Scheme 6: Hydrazone to Azo Conversion of Adduct **I**

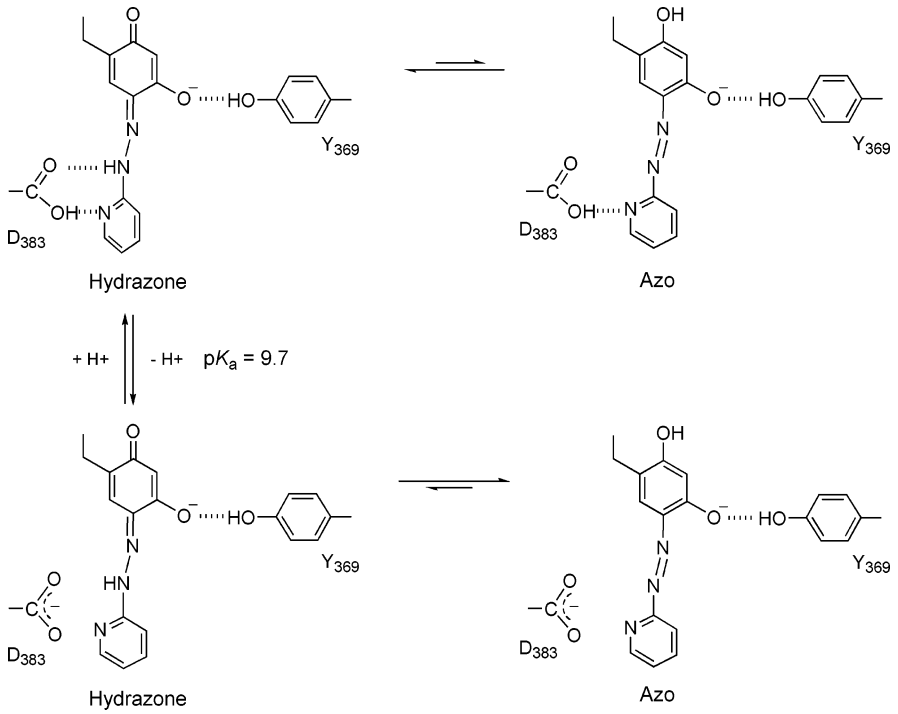

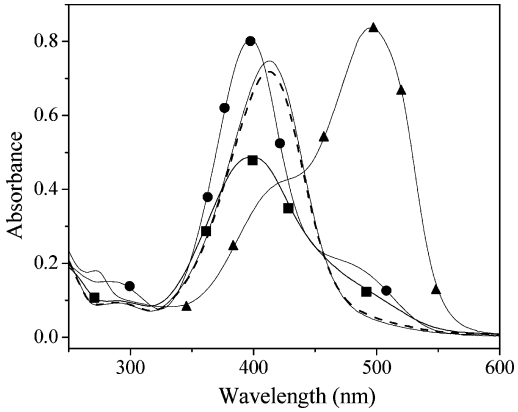

FIGURE 8: Spectral changes of **2** following the addition of **2** in buffers at pH 1.87 (●), 4.42 (■), 7.02 (- - -), 9.78 (—), and 13.38 (▲).

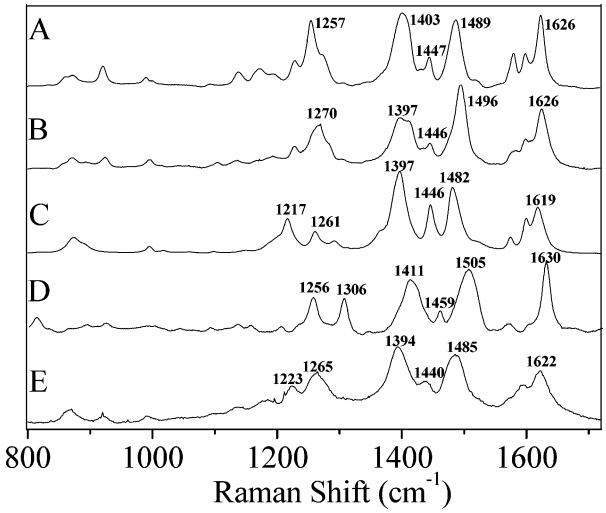

FIGURE 9: Resonance Raman spectra of adduct **I** of (A) D383N, (B) WT-ECAO, (C) **2**, (D) D383E, and (E) AGAO at 413.1 nm excitation wavelength.

tion on adduct **I** of Y369F as this species is unstable and converts to adduct **II** relatively rapidly [see the following paper (*51*)].

UV−Vis Spectroscopic pH Titration of 2. The pK_a values for **2** were determined spectrophotometrically, and the UV−vis absorption spectra of **2** at four different pHs are summarized in Figure 8. An increase in pH from 1.87 to 4.89 resulted in decrease in the absorption band at 398 nm and its associated shoulder at 480 nm. An increase in pH from 4.89 to 9.31 resulted in increase in absorbance at 414 nm and decrease in the band around 500 nm with an isosbestic point around 460 nm. There was no spectral change between pH 9.31 and pH 11.05. Above pH 11.05, the color of the solution changed from yellow to pink, which was due to the appearance of an absorption band at 496 nm and a decrease in absorbance at 414 nm. A plot of A_{398} vs pH in the acidic pH range fits the titration curve for the dissociation of a single proton, allowing the calculation of a pK_a of 2.56 ± 0.08 by least-squares fitting analysis. A pK_a value of 5.92 ± 0.05 was obtained from the plot of A_{414} vs pH. The third pK_a was difficult to determine since the A_{496} did not reach saturation even in 1.0 N NaOH. Plots of A_{414} vs pH and A_{496} vs pH fit the titration curves for a dissociation of a single proton with an estimated pK_a value of 13.1 ± 0.1.

The first pK_a value of 2.56 ± 0.08 is assigned as that of the pyridine nitrogen (pK_a^1 in Scheme 7). Pyridine has a pK_a of 5.23, but the presence of an electron-withdrawing group adjacent to the pyridine ring significantly lowers the pK_a of the pyridine nitrogen. A similar effect is seen for the amino group of aniline when compared to that of 4-phenylazoaniline (4.62 vs 2.82) (*44*). The second pK_a value of 5.92 ± 0.05 is assigned to the 2-hydroxyl group of the TPQ ring (pK_a^2 in Scheme 7). The third pK_a value of 13.1 ± 0.1 is assigned as that of the 4-hydroxyl group (pK_a^3 in Scheme 7). The internal hydrogen-bonding interaction between O4 and N1 of **2** should increase the pK_a of the 4-hydroxyl group significantly. The pK_a values for 2-hydroxyl and 4-hydroxyl groups are in good agreement with those of the phenylhydrazine adduct of **1** (5.93 ± 0.03 and 12.83 ± 0.17, respectively) (*28*).

rR Spectroscopy on Adduct I. Examination of the 2HP adducts of several amine oxidases reveals that λ_{max} of the 2HP adduct ranges from ~415 to 440 nm, indicating that the principal electronic transitions are sensitive to the active site microenvironment and therefore that λ_{max}, by itself, cannot be a definitive indicator of the nature of the 2HP adduct. It is likely that the transitions of the hydrazone tautomer are more sensitive to the active site environment than the delocalized $\pi-\pi^*$ transitions of the azo form. Consequently, the rR spectra are a more reliable indicator of the nature of the 2HP adduct (azo, hydrazone, or mixture) than is λ_{max}. Comparisons between the rR spectra of the proteins and **2** proved very useful in elucidating the chemical and structural nature of adduct **I** of WT-ECAO and the corresponding active site mutants. Figure 9 compares the rR spectra of adduct **I** in WT-ECAO, **2**, and the D383N and D383E variants. Vibrational bands characteristic of bending and stretching modes of the 2HP-derivatized TPQ dominate the 1200−1650 cm^{-1} region. When the excitation wavelength is 413.1 nm as in Figure 9, the WT-ECAO and D383N spectra are broadly similar to the spectrum of **2**. Essentially identical spectra are observed with 457.9 nm excitation. Three vibrational bands between 1575 and ~1626 cm^{-1} are apparent along with three other vibrational bands between 1397 and ~1496 cm^{-1}. The C═N stretching modes of phenyl-substituted hydrazones can be correlated to a region between 1610 and 1630 cm^{-1}, whereas N═N stretching frequencies can be observed between 1380 and 1463 cm^{-1}

Scheme 7: pK_as of **2**

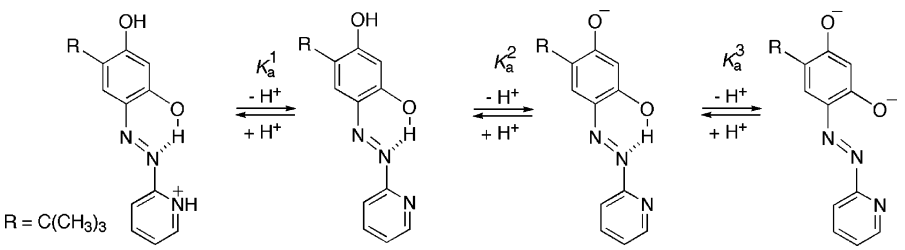

(*48*). A strong vibration at 1442 cm^{-1} has been identified as the N═N stretch in *trans* phenyl-substituted azo compounds (*48*). We assign the ~1446 cm^{-1} observed in the rR spectra of WT-ECAO, D383N, and **2** as the N═N stretch. Further, the overall similarities of the spectra of **2**, WT-ECAO, and D383N suggest that the azo tautomer of these protein derivatives is present in significant amounts in solution. However, the somewhat higher frequency of the highest energy band (1626 vs 1619 cm^{-1}) and the broadening of the ~1400 cm^{-1} feature in the protein spectra suggest that the hydrazone tautomer also contributes. In the rR spectrum of D383E (Figure 9D), the differences with the spectrum of **2** are much more striking. A prominent vibrational band at 1630 cm^{-1} and a more intense band at 1306 cm^{-1} are observed; moreover, the bands between 1400 and ~1500 cm^{-1} are broader and shifted to higher energy in the D383E rR spectrum. Note that the 1446 cm^{-1} mode is absent in the spectrum of D383E. Consequently, the dominant species in the D383E adduct is likely the hydrazone tautomer. Recall that the D383E variant also displayed the lowest energy electronic transition. As a test of these assignments, we have measured the rR spectrum of the 2HP adduct of *A. globiformis* amine oxidase (AGAO), for which adduct **I** displays a $\lambda_{max} \approx 420$ nm. As shown in Figure 9E, the rR spectra of AGAO adduct **I** and **2** are closely similar. Collectively, these data, together with the differences observed in electronic spectra, demonstrate that adduct **I** has more than one conformation. The most straightforward interpretation consistent with all of the data is that in solution adduct **I** exists either as the hydrazone (e.g., D383E), or the azo (**2**), or as a mixture of the two tautomers (WT-ECAO and D383N).

DISCUSSION

Both the solution and the X-ray structural data suggest that **2** exists predominantly as the azo form with the pyridine and TPQ rings being coplanar and in a *trans* configuration. In solution, the azo form is in rapid equilibrium with the hydrazone tautomer, where the equilibrium greatly favors the former. All reported aromatic hydrazones analogous to **2** follow this pattern (*45*). The stabilization of the azo tautomer comes from the extended π-conjugation between the two rings via the azo (N═N) bond. At neutral pH, **2** is a monoanion, where the 2-hydroxyl group is deprotonated and the 4-hydroxyl group is protonated and participates in a strong hydrogen-bonding interaction with the N2 of the azo group to further stabilize this tautomer. Compound **2** adopts a geometry that allows for an intramolecular H-bonding interaction that is precluded in the enzyme active site. Unlike **2**, the hydrazone−azo tautomerism in the enzyme is thus a true equilibrium. Despite these differences, the spectral characteristics of **2** serve as a basis to understand the nature of adduct **I** in ECAO.

In contrast to **2**, adduct **I** of WT-ECAO in the crystal form exists predominantly as the hydrazone form with the two aromatic rings being out of plane relative to one another (70° angle) (see Figures 1B and 5A) (*38*). There are two important hydrogen-bonding interactions that keep the rings in this thermodynamically unfavorable configuration. One is between D383 (protonated) and the pyridine nitrogen of the 2HP moiety and the other is between Y369 and the 4-oxoanion of the TPQ moiety. As a result, the π-conjugation observed in **2** is not present, and the bond between N1 and N2 has more single bond character. From the protein structure, it can be predicted that breaking these two hydrogen bonds should shift the equilibrium toward the azo tautomer. The hydrogen bond between D383 and the pyridine nitrogen of the 2HP moiety also serves to rotate the pyridine ring 180° in WT-ECAO as compared to **2**.

In solution, adduct **I** of WT-ECAO has a λ_{max} which is red shifted and less intense (smaller ϵ value) when compared to **2**. On the basis of the X-ray crystal structure study and rR data (see below), we interpreted these spectral differences as an indication that adduct **I** exists as a tautomeric mixture where the hydrazone form is favored over the azo form in the crystal. UV−vis and rR spectra of adduct **I** in the wild-type and mutant forms of ECAO could be used to indicate the position of the hydrazone/azo equilibrium occupied by TPQ−2HP in solution. A red shift in the λ_{max} when compared to **2** shows an increasing contribution from the hydrazone tautomer.

As shown in Figure 6, we observed a pH-dependent shift in the λ_{max} of WT adduct **I**, yielding a single pK_a of 9.70 ± 0.15, where the UV−vis spectrum of the deprotonated form resembles **2**. This pK_a was assigned to the carboxyl group of D383, where deprotonation disrupts the hydrogen-bonding interaction with the pyridine nitrogen of the 2HP moiety. At elevated pH values, the pyridine ring is free to rotate to be in plane with the TPQ ring, enabling the extended π-conjugated system of the azo tautomer (Scheme 6). This pK_a is absent in **2** (Scheme 7), showing that it is not intrinsic to TPQ−2HP but rather must originate in the enzyme active site. To support this assignment, a similar pH titration was performed on the phenylhydrazone adduct of WT-ECAO which lacks the pyridine nitrogen. As expected, no spectral change was observed over the pH range studied (pH 6−10). No spectral changes were observed in the active site base mutants, D383N and D383E. In D383N, there is no titratable proton. The hydrogen-bonding interaction between the amide group of the N383 and the pyridine nitrogen of the 2HP stabilizes the hydrazone form over the azo form. In D383E, the extra methylene group strengthens the hydrogen-bonding interaction to elevate the pK_a of the carboxyl group.

Pertubations of the hydrogen-bonding interactions can influence the hydrazone/azo tautomeric equilibrium. For example, in D383E, the hydrazone−azo equilibrium of adduct **I** is shifted to the hydrazone tautomer as indicated by the UV−vis and rR spectra. Effects of the hydrogen-bonding interactions were probed by denaturing adduct **I** with 8 M urea (Figure 7). Following the treatment of urea in WT-ECAO, D383N, and D383E, the UV−vis spectra changed immediately, resulting in the blue shift of the λ_{max} to yield the species very similar to the WT-ECAO at pH >9 and **2** at pH 7.

The rR spectra of adduct **I** in WT-ECAO, D383 mutants, and **2** (Figure 9) provide direct evidence that adduct **I** can exist as a mixture of the hydrazo−azo tautomers. In the case of D383N, the hydrazone is present in substantial amounts as indicated by the UV−vis spectral changes (Figure 7). However, the rR spectrum is consistent with a mixture of both hydrazone and azo tautomers. It is possible that the rR spectrum represents an overestimate of the azo population due to a photoinduced conformational change from laser irradiation. WT-ECAO and D383N appear to be very similar to one another but have noticeable differences compared to

Scheme 8: Reductive Half-Reaction of CAOs

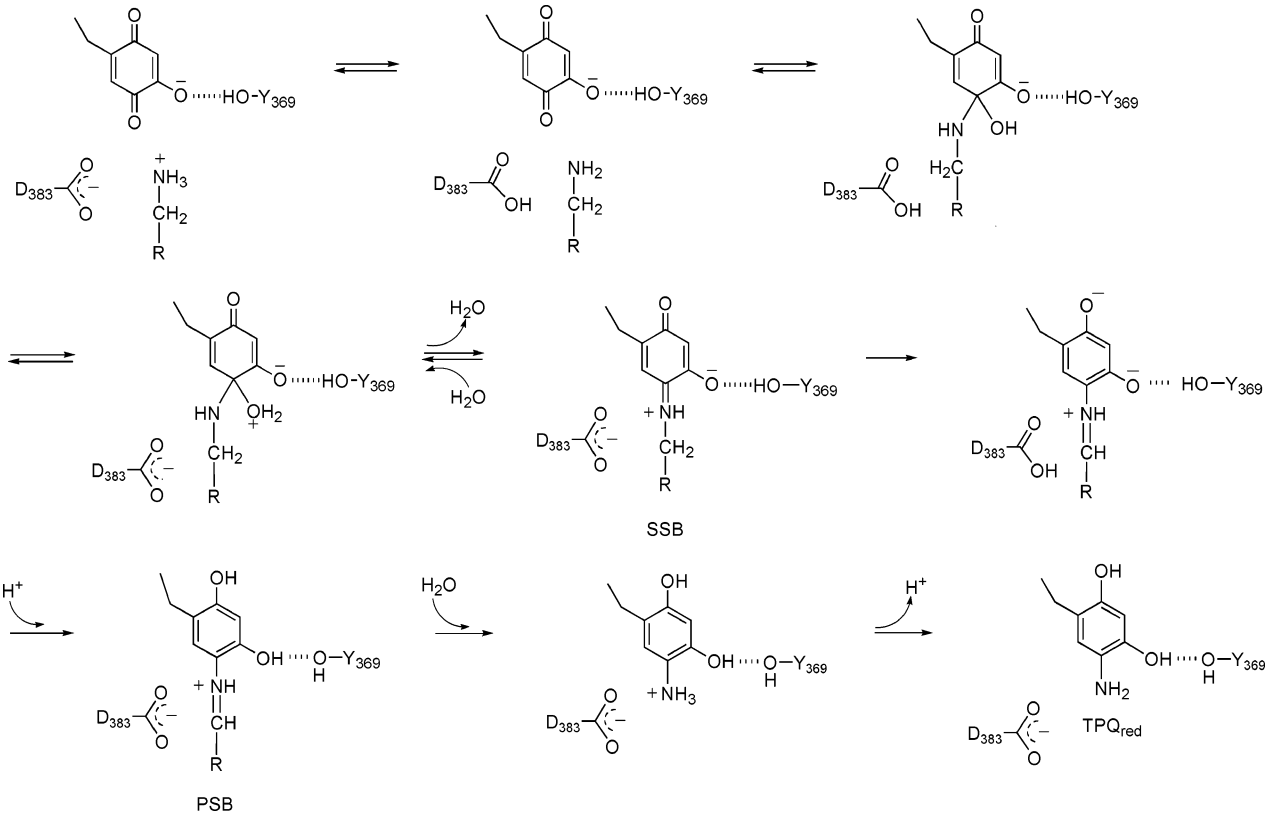

2 and significant differences compared to D383E. The rR spectrum of **2** is not significantly altered as the excitation wavelength is changed from 413.1 to 457.9 nm. This is expected from both the NMR and X-ray crystal structure data, which strongly indicate that **2** exists predominantly as the azo tautomer. Based on the comparison with **2**, it is most likely that D383E exists predominantly as the hydrazone form. On the other hand, in solution WT and D383N contain significant populations of both the hydrazone and azo forms. For other CAOs, the general phenomenon that adduct **I** can exist as a hydrazone, an azo, or a mixture of both is thought to be similar. In the case of AGAO-2HP adduct **I**, the UV−vis spectrum (λ_{max} = 420 nm) and the rR spectrum (Figure 9E) closely resemble those of **2**, suggesting that this adduct is predominantly azo. To support this, we did not observe any changes in the UV−vis spectrum of AGAO-adduct **I** between pH 7 and pH 10. The hydrogen-bonding interaction between the active site base and the 2HP moiety of adduct **I** appears to be absent in AGAO. Further structural characterization of AGAO−adduct **I** will be required to confirm this.

The importance of the hydrogen bond between Y369 and the 4-oxoanion of TPQ was studied by mutating the tyrosine to phenylalanine. This residue plays an important role in catalysis by maintaining TPQ in an active conformation (*18*, *19*). Mutants of Y369 without hydrogen-bonding capabilities show a disordered structure with respect to TPQ (*18*), demonstrating increased mobility of TPQ in the active site compared to WT-ECAO. As a result, it was expected that adduct **I** in these mutants would favor the azo form as the TPQ ring should be free to be coplanar with the hydrogen-bonded pyridine ring of the 2HP moiety. Consistent with this expectation, the λ_{max} of adduct **I** of Y369F is similar to λ_{max} of **2** at neutral pH and λ_{max} of WT-ECAO (at higher pH). However, adduct **I** of Y369F was not stable and converted to adduct **II**, the nature of which will be discussed in the following paper (*51*). Suffice to say here that the structure of adduct **II** requires the azo tautomeric form.

The formation of **2** in aqueous solution at physiological pH occurs via general acid catalysis (Scheme 4). In ECAO, D383 plays an important role to facilitate adduct **I** formation prior to stabilizing the hydrazone tautomer of adduct **I**, as discussed above. The proposed mechanism for formation of adduct **I** in WT-ECAO is shown Scheme 3. When 2HP binds to the active site as its protonated form (pK_a = 8.07), the deprotonated D383 (pK_a = 5.81) picks up the proton to facilitate the nucleophilic addition of 2HP to the C5 carbonyl carbon of TPQ, thereby forming the first, carbinolamine-like, intermediate. Subsequently, the protonated D383 donates the proton back to this intermediate to catalyze the dehydration reaction, yielding adduct **I**. In contrast to the imino nitrogen of the substrate Schiff base intermediate, the pK_a of the N1 of the hydrazone (azo) group is significantly acidic [cf. pK_a = −0.28 for 4-phenylazo-6-*tert*-butylresorcinol (*49*)] so that the proton on N1 will be released rapidly to form adduct **I** as a monoanion. The proton so released is then taken back up by D383. This role for the active site base as a proton sink has been proposed in the catalytic mechanism of HPAO (see Scheme 8) (*24*). The crystal structure of ECAO−2HP adduct **I** suggests that there is a hydrogen-bonding interaction between the pyridine nitrogen of 2HP and D383. Previously, it was unclear whether the proton resided on the pyridine nitrogen or D383 (*38*). However, as the pK_a of the pyridine nitrogen of **2** in an aqueous solution is 2.56 ± 0.08, it is now clear that D383 is protonated following the formation of adduct **I**.

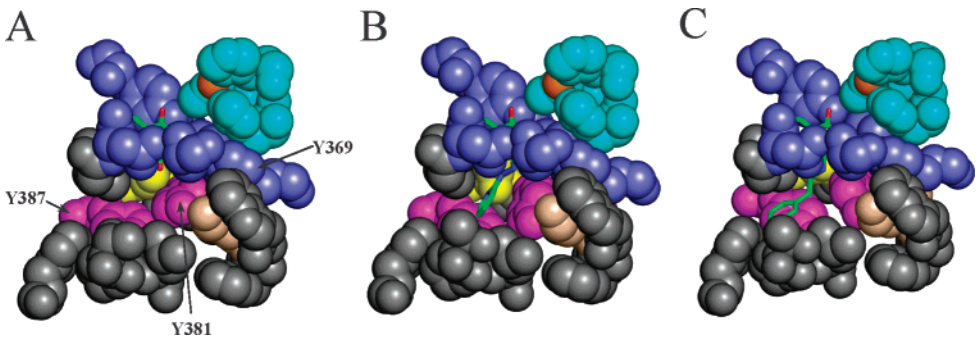

FIGURE 10: Hydrophobic cavity in the active site. (A) WT-ECAO, resting form. (B) WT-ECAO adduct **I**. (C) WT-ECAO TCP adduct (1LVN.pdb). Hydrophobic residues are shown in gray spheres. TPQ is shown in stick representation where the O2 and O5 carbonyl groups are shown in red. D383 is shown in yellow spheres. Y381 and Y387 are shown as magenta spheres. Residues that form the wedge-shaped cavity around TPQ are shown as slate blue spheres including Y369 (*16*, *17*). K379 is shown in tan spheres. Cu is shown as an orange sphere, and histidine residues are shown as aqua spheres. Figures are generated by Pymol (DeLano Scientific LLC, http//www.pymol.org).

In a prior study, adduct **I** was proposed to mimic the structure of the SSB intermediate in the catalytic cycle (see Scheme 2) (*36*). Via UV−vis spectroscopy and comparisons to the corresponding model compounds, the SSB was determined to exist as a zwitterion with the protonated imine nitrogen and the 4-oxoanion of TPQ (*25*). The active site base (deprotonated) abstracts the C1 proton from the intermediate to undergo catalysis (Scheme 8). Similarly, in the previous proposal (*36*), N1 of adduct **I** is protonated and the 4-hydroxyl group of TPQ is deprotonated (Scheme 2). This model also required that D383 is deprotonated to catalyze the tautomerization to the azo form. However, in the present study, we have shown that D383 is protonated in the adduct **I** form of the enzyme due to the acidity of the N1 of adduct **I** and that the position of the equilibrium between the hydrazone and azo tautomers is controlled by the protonation state of D383.

In WT-ECAO adduct **I**, the interaction between D383 and the 2HP moiety should keep adduct **I** predominantly in the hydrazone conformation where the N2 is *cis* to C4 of the TPQ ring. This interaction is not present in the SSB complex, and yet ECAO is still able to specifically direct the α-proton abstraction by D383. This step is highly stereoselective, favoring the *pro-S* proton over the *pro-R* proton in ECAO (*38*). A comparison between the structures of **2** and WT-ECAO adduct **I** suggests that the active site of ECAO is able to specifically orient the SSB.

In contrast to WT-ECAO adduct **I**, in **2** N2 is *trans* to C4 of the TPQ ring due to the intramolecular hydrogen-bonding interaction between the 4-hydroxyl group and N2. A closer inspection of the active site structure of WT-ECAO adduct **I** reveals that, even upon conversion to the azo form by breaking the hydrogen-bonding interactions with D383, adduct **I** likely cannot adopt a conformation analogous to **2** without some rearrangement in the active site, due to the steric bulk of Y381 and the surrounding hydrophobic residues (see Figure 10A). There is a hydrophobic cavity (defined by F192, T223, P224, L225, W257, Y381, Y387, V463, and G464) that appears to be the substrate binding pocket, where this cavity can be seen clearly in WT-ECAO (Figure 10B) and the TCP-inhibited form of ECAO (Figure 10C). By extension, the SSB complex must adopt a conformation similar to that of adduct **I** and the TCP-inhibited form, and this is how ECAO can direct the α-proton abstraction of the SSB complex by D383. Comparison of the active site structures of the adduct **I** forms of ECAO and other CAOs will help to clarify the origin of the specificity of the α-proton abstraction step.

CONCLUSIONS

In the course of this study, we have now fully characterized adduct **I** in ECAO. In WT-ECAO, adduct **I** exists as a tautomeric mixture where the hydrazone form predominates over the azo form. This is in stark contrast to the solution chemistry where the model compound, **2**, exists predominantly as the azo form. The protein adduct **I** is an unusual example of an aromatic hydrazone having greater stability than the azo form. D383 and Y369, which are active site residues intimately involved in the catalytic cycle of CAOs, stabilize the hydrazone form via specific hydrogen-bonding interactions. In D383E, we have shown that the hydrogen-bonding interaction between the carboxyl group and the pyridine nitrogen of TPQ-2HP is strengthened when compared to that in WT-ECAO. A steric effect of the D to E mutation was originally indicated from the crystal structure analysis of D383E, where the mobility of TPQ in the active site was greatly reduced. The present result is further direct evidence that the D to E mutation affects critical interactions within the active site, thereby explaining the greatly reduced activity of D383E.

Although adduct **I** has some similarities to the SSB in the catalytic cycle (Scheme 8), there are important differences. D383 in adduct **I** is protonated (Scheme 3), but it is deprotonated in the SSB (Scheme 8) (*24*, *50*). Further, the SSB is net neutral (Scheme 8) whereas adduct **I** is monoanionic (Scheme 3). Despite these differences, adduct **I** does provide key structural insights into how the active site orients the SSB for optimal activity. In addition, we have shown that adduct **I** comprises both hydrazone and azo tautomers. This means that adduct **II** is not the azo tautomer as previously proposed. In the following paper (*51*), we will discuss the surprising nature of adduct **II** of ECAO.

ACKNOWLEDGMENT

We thank Pierre Möenne-Loccoz at the Oregon Graduate Institute for technical assistance with some of the resonance Raman experiments. We also thank Takanori Tanaka at ISIR, Osaka University, Japan, for X-ray crystal structural analysis of **2** and David Vander Velde and Sarah Neuenswander for

helpful discussions regarding ^{15}N NMR spectroscopy. M.M. thanks Judith Klinman and Katsuyuki Tanizawa for providing support for M.M. to work on this project and also Julian Limburg for critical reading of the manuscript and valuable discussions.

SUPPORTING INFORMATION AVAILABLE

Kinetic determination of the pK_a for the formation of **2** (Figure S1), spectroscopic determination of the pK_as of 2HP (Figure S2), and experimental details for the X-ray structure determination of **2** and details concerning the pK_a assignment of 2HP by ^1H and ^{15}N NMR spectroscopy. This material is available free of charge via the Internet at http://pubs.acs.org.

REFERENCES

1. McIntire, W. S. (1998) Newly discovered redox cofactors: Possible nutritional, medical, and pharmacological relevance to higher animals, *Annu. Rev. Nutr. 18*, 145−177.
2. Dooley, D. M., and McGuirl, M. A. (1986) Spectroscopic studies of pig kidney diamine oxidase-anion complexes, *Inorg. Chim. Acta 123*, 231−236.
3. Rea, G., Metoui, O., Infantino, A., Federico, R., and Angelini, R. (2002) Copper amine oxidase expression in defense responses to wounding and *Ascochyta rabiei* invasion, *Plant Physiol. 128*, 865−875.
4. Elmore, B., Bollinger, J. A., and Dooley, D. M. (2002) Human kidney diamine oxidase: Heterologous expression, purification, and characterization, *J. Biol. Inorg. Chem. 7*, 565−579.
5. Jalkanen, S., and Salmi, M. (2001) Cell surface monoamine oxidases: Enzymes in search of a function, *EMBO J. 20*, 3893−3901.
6. Janes, S. M., Mu, D., Wemmer, D., Smith, A. J., Kaur, S., Maltby, D., Burlingame, A. L., and Klinman, J. P. (1990) A new redox cofactor in eukaryotic enzymes: 6-Hydroxydopa at the active site of bovine serum amine oxidase, *Science 248*, 981−987.
7. Matsuzaki, R., Fukui, T., Sato, H., Ozaki, Y., and Tanizawa, K. (1994) Generation of the topa quinone cofactor in bacterial monoamine oxidase by cupric ion-dependent autooxidation of a specific tyrosyl residue, *FEBS Lett. 351*, 360−364.
8. Cai, D., and Klinman, J. P. (1994) Evidence for a self-catalytic mechanism of 2,4,5-trihydroxyphenylalanine quinone biogenesis in yeast copper amine oxidase, *J. Biol Chem. 269*, 32039−32042.
9. Ruggiero, C. E., Smith, J. A., Tanizawa, K., and Dooley, D. M. (1997) Mechanistic studies of topa quinone biogenesis in phenylethylamine oxidase, *Biochemistry 36*, 1953−1959.
10. Parsons, M. R., Convery, M. A., Wilmot, C. M., Yadav, K. D. S., Blakeley, V., Corner, A. S., Phillips, S. E. V., McPherson, M. J., and Knowles, P. F. (1995) Crystal structure of a quinoenzyme: Copper amine oxidase of *Escherichia coli* at 2 Å resolution, *Structure 3*, 1171−1184.
11. Wilce, M. C. J., Dooley, D. M., Freeman, H. C., Guss, J. M., Matsunami, H., McIntire, W. S., Ruggiero, C. E., Tanizawa, K., and Yamaguchi, H. (1997) Crystal structures of the copper-containing amine oxidase from *Arthrobacter globiformis* in the holo and apo forms: Implications for the biogenesis of topaquinone, *Biochemistry 36*, 16116−16133.
12. Li, R. B., Klinman, J. P., and Mathews, F. S. (1998) Copper amine oxidase from *Hansenula polymorpha*: The crystal structure determined at 2.4 Å resolution reveals the active conformation, *Structure 6*, 293−307.
13. Lee, M., Willingham, K., Langley, D., Maher, M. J., Cohen, A. E., Ellis, P. J., Kuchar, J. A., Dooley, D. M., Freeman, H. C., and Guss, J. M. (2002) Crystallization of *Pichia pastoris* lysyl oxidase, *Acta Crystallogr., D: Biol. Crystallogr. 58*, 2177−2179.
14. Duff, A. P., Cohen, A. E., Ellis, P. J., Kuchar, J. A., Langley, D. B., Shepard, E. M., Dooley, D. M., Freeman, H. C., and Guss, J. M. (2003) The crystal structure of *Pichia pastoris* lysyl oxidase, *Biochemistry 42*, 15148−15157.
15. Kumar, V., Dooley, D. M., Freeman, H. C., Guss, J. M., Harvey, I., McGuirl, M. A., Wilce, M. C. J., and Zubak, V. M. (1996) Crystal structure of a eukaryotic (pea seedling) copper-containing amine oxidase at 2.2 Å resolution, *Structure 4*, 943−955.
16. Mure, M. (2004) Tyrosine-derived quinone cofactors, *Acc. Chem. Res. 37*, 131−139.
17. Murray, J. M., Saysell, C. G., Wilmot, C. M., Tambyrajah, W. S., Jaeger, J., Knowles, P. F., Phillips, S. E. V., and McPherson, M. J. (1999) The active site base controls cofactor reactivity in *Escherichia coli* amine oxidase: X-ray crystallographic studies with mutational variants, *Biochemistry 38*, 8217−8227.
18. Murray, J. M., Kurtis, C. R., Tambyrajah, W., Saysell, C. G., Wilmot, C. M., Parsons, M. R., Phillips, S. E. V., Knowles, P. F., and McPherson, M. J. (2001) Conserved tyrosine-369 in the active site of *Escherichia coli* copper amine oxidase is not essential, *Biochemistry 40*, 12808−12818.
19. Hevel, J. M., Mills, S. A., and Klinman, J. P. (1999) Mutation of a strictly conserved, active-site residue alters substrate specificity and cofactor biogenesis in a copper amine oxidase, *Biochemistry 38*, 3683−3693.
20. Cai, D. Y., Dove, J., Nakamura, N., Sanders-Loehr, J., and Klinman, J. P. (1997) Mechanism-based inactivation of a yeast methylamine oxidase mutant: Implications for the functional role of the consensus sequence surrounding topaquinone, *Biochemistry 36*, 11472−11478.
21. Schwartz, B., Green, E. L., Sanders-Loehr, J., and Klinman, J. P. (1998) Relationship between conserved consensus site residues and the productive conformation for the TPQ cofactor in a copper-containing amine oxidase from yeast, *Biochemistry 37*, 16591−16600.
22. Plastino, J., Green, E. L., Sanders-Loehr, J., and Klinman, J. P. (1999) An unexpected role for the active site base in cofactor orientation and flexibility in the copper amine oxidase from *Hansenula polymorpha*, *Biochemistry 38*, 8204−8216.
23. Green, E. L., Nakamura, N., Dooley, D. M., Klinman, J. P., and Sanders-Loehr, J. (2002) Rates of oxygen and hydrogen exchange as indicators of TPQ cofactor orientation in amine oxidases, *Biochemistry 41*, 687−696.
24. Mure, M., Mills, S. A., and Klinman, J. P. (2002) Catalytic mechanism of the topa quinone containing copper amine oxidases, *Biochemistry 41*, 9269−9278.
25. Shepard, E. M., Smith, J., Elmore, B., Kuchar, J. A., Sayre, L. M., and Dooley, D. M. (2002) Towards the development of selective amine oxidase inhibitors. Mechanism-based inhibition of six copper containing amine oxidases, *Eur. J. Biochem. 269*, 3645−3658.
26. Klinman, J. P. (2003) The multi-functional topa-quinone copper amine oxidases, *Biochim. Biophys. Acta 1647*, 131−137.
27. Janes, S. M., Palcic, M. M., Scaman, C. H., Smith, A. J., Brown, D. E., Dooley, D. M., Mure, M., and Klinman, J. P. (1992) Identification of topaquinone and its consensus sequence in copper amine oxidases, *Biochemistry 31*, 12147−12154.
28. Mure, M., and Klinman, J. P. (1993) Synthesis and spectroscopic characterization of model compounds for the active site cofactor in copper amine oxidases, *J. Am. Chem. Soc. 115*, 7117−7127.
29. Mure, M., and Klinman, J. P. (1995) Model studies of topaquinone-dependent amine oxidases. 2. Characterization of reaction intermediates and mechanism, *J. Am. Chem Soc. 117*, 8707−8718.
30. Janes, S. M., and Klinman, J. P. (1991) An investigation of bovine serum amine oxidase active site stoichiometry: Evidence for an aminotransferase mechanism involving two carbonyl cofactors per enzyme dimer, *Biochemistry 30*, 4599−4605.
31. Morpurgo, L., Agostinelli, E., Mondovi, B., Avigliano, L., Silvestri, R., Stefancich, G., and Artico, M. (1992) Bovine serum amine oxidase: Half-site reactivity with phenylhydrazine, semicarbazide, and aromatic hydrazides, *Biochemistry 31*, 2615−2621.
32. Brown, D. E., McGuirl, M. A., Dooley, D. M., Janes, S. M., Mu, D., and Klinman, J. P. (1991) The organic functional group in copper-containing amine oxidases. Resonance Raman spectra are consistent with the presence of topa quinone (6-hydroxydopa quinone) in the active site, *J. Biol. Chem. 266*, 4049−4051.
33. Collison, D., Knowles, P. F., Mabbs, F. E., Rius, F. X., Singh, I., Dooley, D. M., Cote, C. E., and McGuirl, M. (1989) Studies on the active site of pig plasma amine oxidase, *Biochem. J. 264*, 663−669.
34. Knowles, P. F., Singh, I., Yadav, K. D. S., Mabbs, F. E., Collison, D., Cote, C. E., Dooley, D. M., and McGuirl, M. A. (1989) Active site structures of copper-containing oxidases, in *PQQ and Quinoproteins* (Jonegan, J. A. D., and Duine, J. A., Eds.) pp 283−288, Kluwer Academic Publishers, Dordrecht.
35. Dooley, D. M., Cote, C. E., McGuirl, M. A., Bates, J. L., Perkins, J. B., Moog, R. S., Singh, I., Knowles, P. F., and McIntire, W. S. (1989) Copper-PQQ interactions in amine oxidases, in *PQQ and Quinoproteins* (Jongejan, J. A., and Duine, J. A., Eds.) pp 307−316, Kluwer Academic Publishers, Dordrecht.

36. Saysell, C. G., Murray, J. M., Wilmot, C. M., Brown, D. E., Dooley, D. M., Phillips, S. E. V., McPherson, M. J., and Knowles, P. F. (2000) Investigation into the mechanism of lamda max shifts and their dependence on pH for the 2-hydrazinopyridine derivatives of two copper amine oxidases, *J. Mol. Catal. B 8*, 17−25.
37. De Matteis, G., Agostinelli, E., Mondovi, B., and Morpurgo, L. (1999) The metal function in the reactions of bovine serum amine oxidase with substrates and hydrazine inhibitors, *J. Biol. Inorg. Chem. 4*, 348−353.
38. Wilmot, C. M., Murray, J. M., Alton, G., Parsons, M. R., Convery, M. A., Blakeley, V., Corner, A. S., Palcic, M. M., Knowles, P. F., McPherson, M. J., and Phillips, S. E. V. (1997) Catalytic mechanism of the quinoenzyme amine oxidase from *Escherichia coli*: Exploring the reductive half-reaction, *Biochemistry 36*, 1608−1620.
39. Saysell, C. G., Tambyrajah, W. S., Murray, J. M., Wilmot, C. M., Phillips, S. E. V., McPherson, M. J., and Knowles, P. F. (2002) Probing the catalytic mechanism of *Escherichia coli* amine oxidase using mutational variants and a reversible inhibitor as a substrate analogue, *Biochem. J. 365*, 809−816.
40. Mure, M., and Klinman, J. P. (1995) Model studies of topaquinone-dependent amine oxidases. 1. Oxidation of benzylamine by topaquinone analogs, *J. Am. Chem Soc. 117*, 8698−8706.
41. Sheldrick, G. M. (1985) *Crystallographic Computing* (Sheldrick, G. M., Kruger, C., and Goddard, R., Eds.) pp 175−185, Oxford University Press, Oxford.
42. Beurskens, P. T., Admiraal, G., Beurskens, G., Bosman, W. P., de Gelder, R., Israel, R., and Smits, J. M. M. (1994) The DIRDIF-94 program system, Technical Report of the Crystallography Laboratory, University of Nijmegen, The Netherlands.
43. Molecular Structure Corp. (1985) Crystal Structure Analysis Package.
44. Fasman, G. D., Ed. (1976) *Handbook of Biochemistry and Molecular Biology*, CRC Press, Cleveland, OH.
45. Krueger, P. J. (1975) *The Chemistry of the Hydrazo, Azo, and Azoxy Groups*, John Wiley and Sons, New York.
46. Saeva, F. D. (1971) Tautomeric behaviour comparison of 4-phenylazo-1-napthol and 1-phenylazo-2-napthol systems by nuclear magnetic resonance, *J. Org. Chem 36*, 3842−3843.
47. Schiott, B., Iverson, B. B., Hellerup Madsen, G. K., and Bruice, T. C. (1998) Characterization of the short strong hydrogen bond in benzoylacetone by ab initio calculations and accurate diffraction experiments. Implications for the electronic nature of low-barrier hydrogen bonds in enzymatic reactions, *J. Am. Chem. Soc. 120*, 12117−12124.
48. Lin-Vien, D., Colthup, N., Fateley, W., and Grasselli, J. (1991) *The Handbook of Infrared and Raman Characteristic Frequencies of Organic Molecules*, Academic Press, Boston, MA.
49. Mure, M., Wang, S. X., and Klinman, J. P. (2003) Synthesis and characterization of model compounds of the lysine tyrosyl quinone cofactor of lysyl oxidase, *J. Am. Chem. Soc. 125*, 6113−6125.
50. Farnum, M., Palcic, M., and Klinman, J. P. (1986) pH Dependence of deuterium isotope effects and tritium exchange in the bovine plasma amine oxidase reaction: A role for single-base catalysis in amine oxidation and imine exchange, *Biochemistry 25*, 1898−1904.
51. Mure, M., Kurtis, C. R., Brown, D. E., Rogers, M. S., Tambyrajah, W. S., Saysell, C., Wilmot, C. M., Phillips, S. E. V., Knowles, P. F., Dooley, D. M., and McPherson, M. J. (2005) *Biochemistry 44*, 1583−1594.

BI047988K